OBSERVATIONS AND IMPLICATIONS OF INTERGRANULAR STRESS CORROSION CRACK GROWTH OF ALLOY 152 WELD METALS IN SIMULATED PWR PRIMARY WATER

Mychailo B. Toloczko, Matthew J. Olszta, Nicole J. Overman, and Stephen M. Bruemmer
Pacific Northwest National Laboratory, Richland, WA 99352

ABSTRACT

Significant intergranular (IG) crack growth during stress corrosion cracking (SCC) tests has been documented during tests in simulated PWR primary water on two alloy 152 specimens cut from a weldment produced by ANL. The cracking morphology was observed to change from transgranular (TG) to mixed mode (up to ~60% IG) during gentle cycling and cycle + hold loading conditions. Measured crack growth rates under these conditions often suggested a moderate degree of environmental enhancement consistent with faster growth on grain boundaries. However, overall SCC propagation rates at constant stress intensity (K) or constant load were very low in all cases. Initial SCC rates up to $6x10^{-9}$ mm/s were occasionally measured, but constant K/load growth rates dropped below ~$1x10^{-9}$ mm/s with time even when significant IG engagement existed. Direct comparisons were made among loading conditions, measured crack growth response and cracking morphology during each test to assess IGSCC susceptibility of the alloy 152 specimens. These results were analyzed with respect to our previous SCC crack growth rate measurements on alloy 152/52 welds.

Introduction

Alloy 152 is a replacement weld material for alloy 182 and is used for shielded metal arc welding (SMAW) of alloy 690 and dissimilar metal welds. Like alloy 690, it contains ~30% chromium to provide improved stress corrosion resistance. It contains higher levels of some solute elements found in alloy 690 such as Mn, and several other additional solutes not found in alloy 690 such as Nb, Ta, Mo, Ti and Al. Weld grains are typically highly elongated with many having a length reaching 1-2 mm and a width of 250-500 μm in comparison to smaller equiaxed 50-100 μm grains in alloy 690 thick-wall tubing. Dendritic structures are evident within the grains, and small Nb and Cr carbides can be found on the grain and dendrite boundaries. Laboratory testing of the stress corrosion crack growth resistance of alloy 152/52/52M welds in PWR primary water have been ongoing at many laboratories **[1-8]** for more than five years. As shown in Figure 1, reported constant K or constant load (L) crack growth rates (CGRs) have primarily been below $5x10^{-9}$ mm/s, similar to that for tests of non-cold worked alloy 690 **[9]**. Exceptions to these low CGRs were observed by Argonne National Laboratory (ANL) on two different alloy 152 weldments **[5-7]** produced at ANL from the same heat of weld filler metal. Measured constant load CGRs on these weldments were 1-$4x10^{-8}$ mm/s with IG engagement reported to be as high as 95%. As part of a collaborative testing program, ANL has provided slices from one of these weldments to Pacific Northwest National Laboratory (PNNL) and General Electric Global Research (GE) for comparative testing. Testing and analysis performed by PNNL on two specimens extracted from this weldment are described here in an effort to try to clarify the crack growth response.

Disclaimer: The work reported in this paper was supported by the Office of Nuclear Regulatory Research, U.S. Nuclear Regulatory Commission. The views expressed in this paper are not necessary those of the U.S. Nuclear Regulatory Commission.

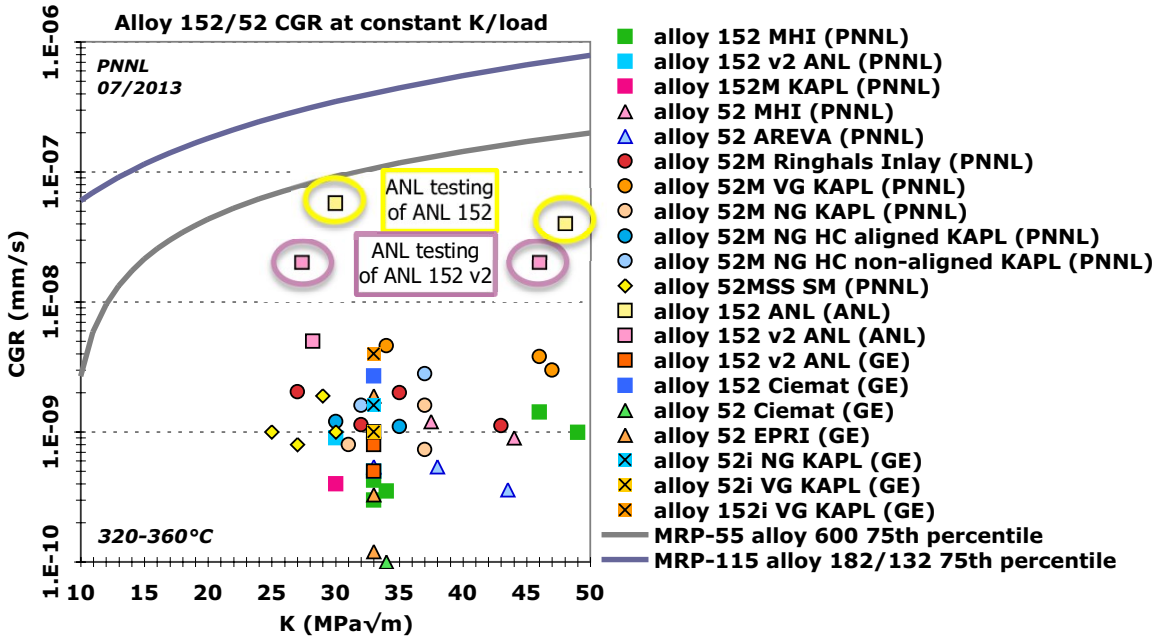

Figure 1. Summary of reported PWSCC constant K or constant load crack growth rates for various alloy 152/52 welds **[1-7]**.

Experimental

Material and Specimens

The composition of the alloy 152 heat WC04F6 weld filler metal used by ANL in their original and new alloy 152 weldment is listed in Table 1. PNNL received slices from the new (second) weldment, and it is referred here as the alloy 152 v2 weld. A diagram provided by ANL of the intended weldment geometry and weld-pass buildup plan is shown in Figure 2. It is a double bevel weld that joins alloy 690 to A533 steel. In preparation for the joint weld, the A533 steel plate was buttered with three layers of alloy 152 (not heat WC04F6), and this buttered A533 plate was given a post-weld heat treatment at 621°C for 3 hours. Due to limited quantities of heat WC04F6 weld filler metal, only a portion of the joint was fabricated using this filler metal. The remaining weld passes were made from two other heats of alloy 152. SCC testing at PNNL was confined to weld passes made from heat WC04F6.

As part of test preparation and during post-test analysis of the specimens, a variety of characterizations were carried out in the region of the WC04F6 weld passes. A rough polish and etch was first applied to the entire weldment as shown in Figure 3. Since stress corrosion cracking (SCC) susceptibility is often scales with material strength, microhardness mapping was performed on the weldment, and as shown in Figure 4, Vickers hardness was found to vary from ~200-260 kg/mm^2. In comparison, microhardness measurements on alloy 690TT, 17%CR alloy 690TT and 31%CR alloy 690TT yielded average values of 175, 240 and 300 kg/mm^2, respectively [9]. Next a variety of optical and scanning electron microscopy (SEM) examinations were performed to characterize boundary structures and compositional variations within the weldment. Figure 5 shows grain boundaries and dendrite boundaries using optical differential imaging contrast, SEM backscatter electron (BSE) imaging, and electron backscatter diffraction (EBSD). Both high angle and low angle grain boundaries were apparent and exhibited different contrast in EBSD imaging while optical imaging tended to detect only high angle grain boundaries. SEM-BSE did not clearly distinguish between high and low angle grain boundaries, but tended to most clearly show the dendritic boundaries.

Table 1. Composition of the alloy 152 heat WC04F6 weld filler metal used by ANL in their original and new alloy 152 weldments. Values are in wt%.

Heat	Cr	Fe	Mn	C	Si	Nb+Ti	Al	Ti	P	S
WC04F6	28.7	10.4	3.5	0.048	0.41	1.54	0.06	0.09	0.003	0.003

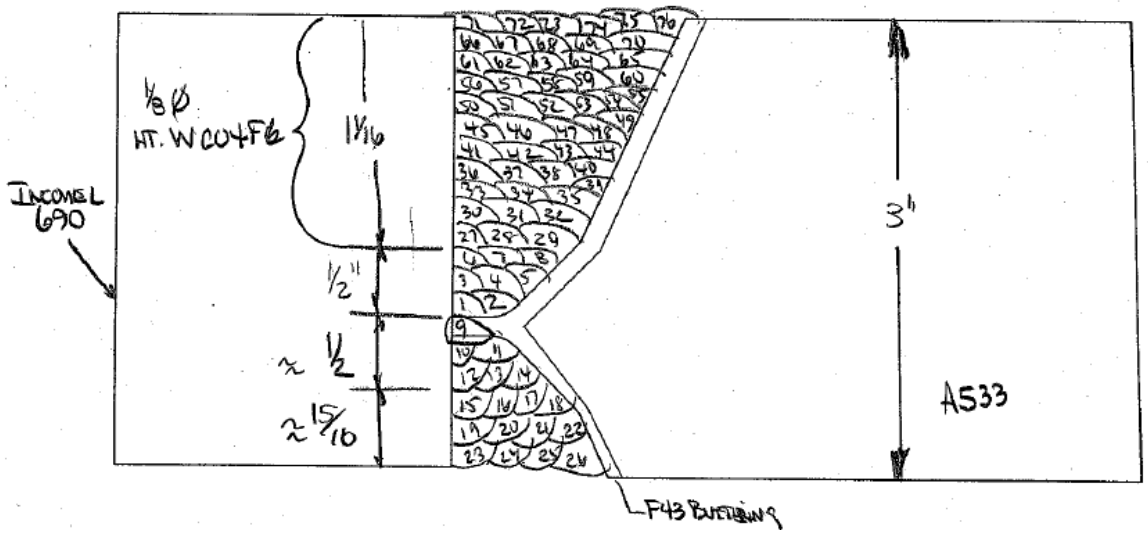

Figure 2. Weld buildup plan for the "new" alloy 152 weldment fabricated by ANL **[7]** using alloy 152 heat WC04F6. PNNL has been using the name "alloy 152 v2" for this weldment.

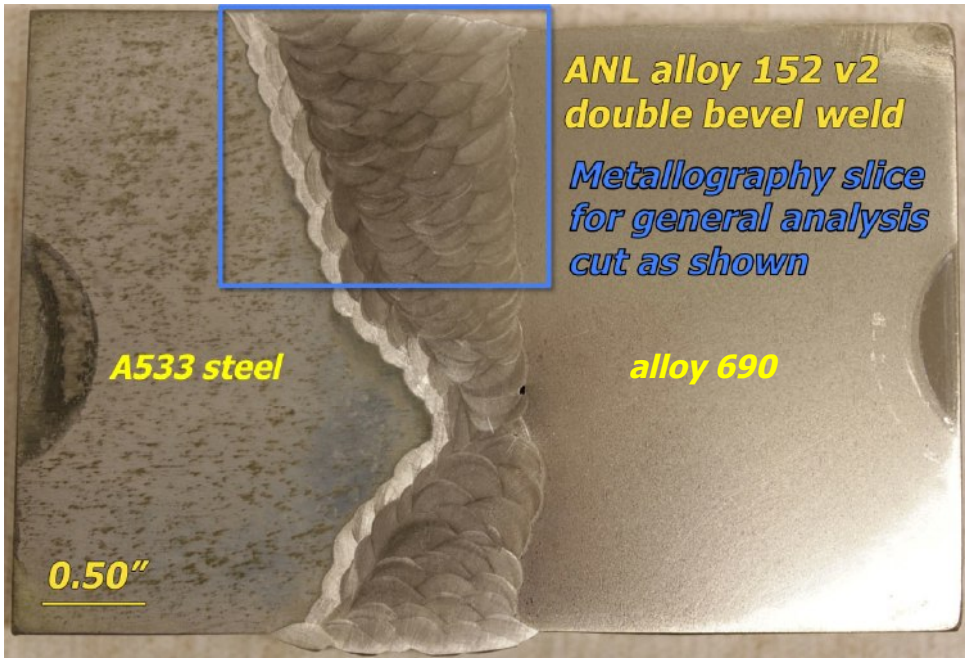

Figure 3. Optical macro image of a weld slice taken from the ANL alloy 152v2 weldment. Note that the weld orientation is flipped from drawing in Figure 2. Blue box indicates the WC04F6 weld region examined in more detail.

Disclaimer: The work reported in this paper was supported by the Office of Nuclear Regulatory Research, U.S. Nuclear Regulatory Commission. The views expressed in this paper are not necessary those of the U.S. Nuclear Regulatory Commission.

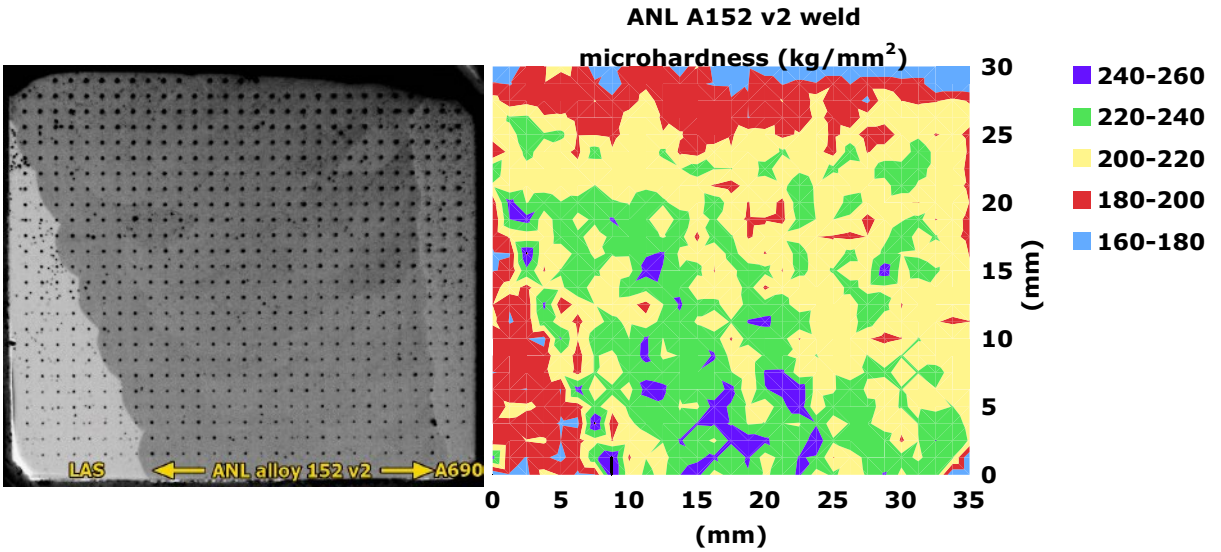

Figure 4. Microhardness indent pattern and resulting hardness map for the macro slice of the WC04F6 weld region. Slightly higher hardness (green to blue) is indicated in the alloy 152 v2 weld metal near the butter layers that were applied to the A533 low alloy steel (LAS).

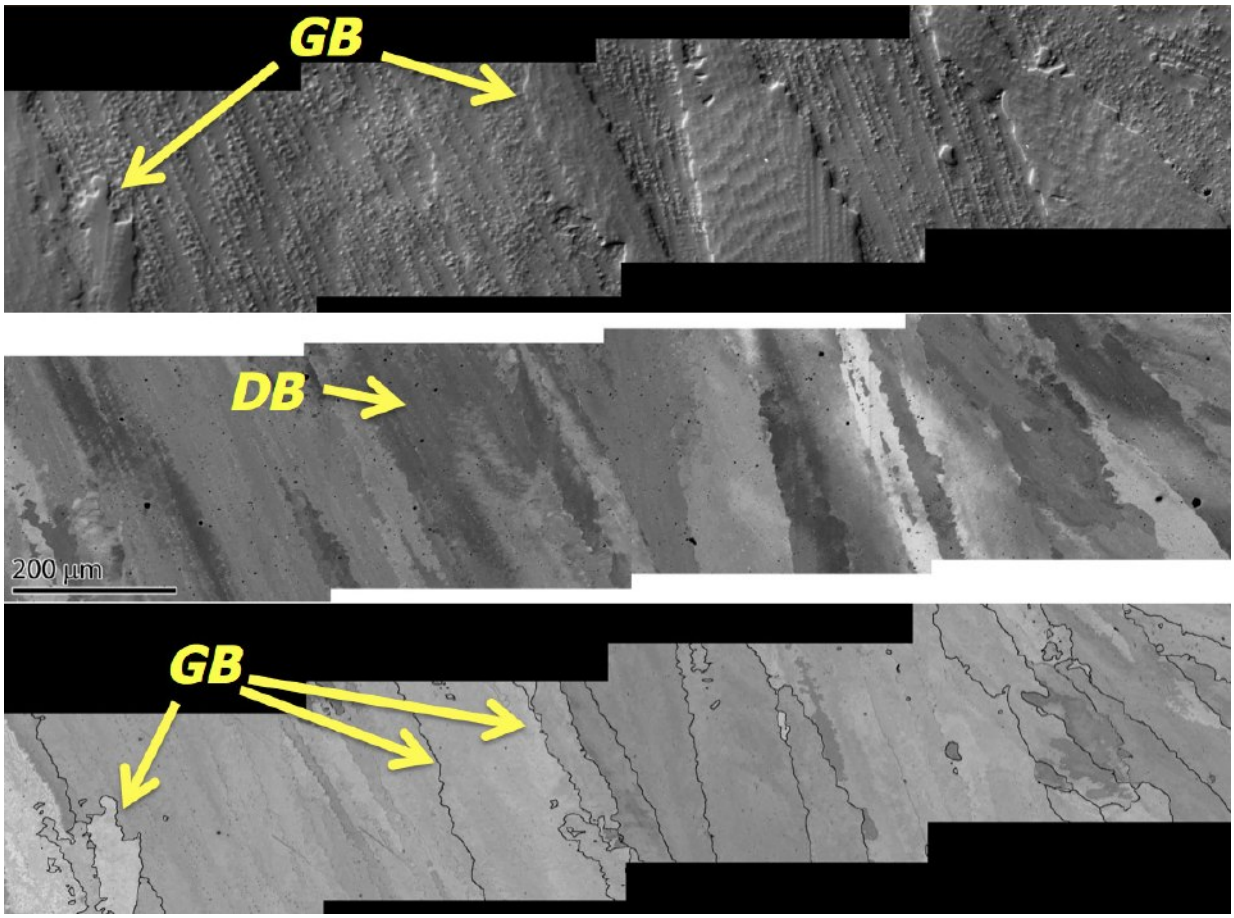

Figure 5. Comparison of grain (GB) and dendrite boundary (DB) structures of the alloy 152 v2 weldment using optical imaging (top), SEM-BSE imaging (middle), and EBSD pattern quality map (bottom).

Both lower (Figure 6) and higher (Figure 7) magnification SEM energy dispersive spectrometry (EDS) imaging of spatial elemental distribution was performed. The low magnification images indicate variations in Mn and Nb content consistent with the size and shape of the dendritic fingers. These EDS maps also showed a low density of Al- and Ti-containing particles dispersed throughout the matrix. Higher magnification images revealed Nb- and Cr-rich carbides of the order of 50-100 nm decorating high-angle grain boundaries, while only NbC was found on the dendritic boundaries. These elemental distributions are similar to other alloy 152 weldments that have been characterized at PNNL.

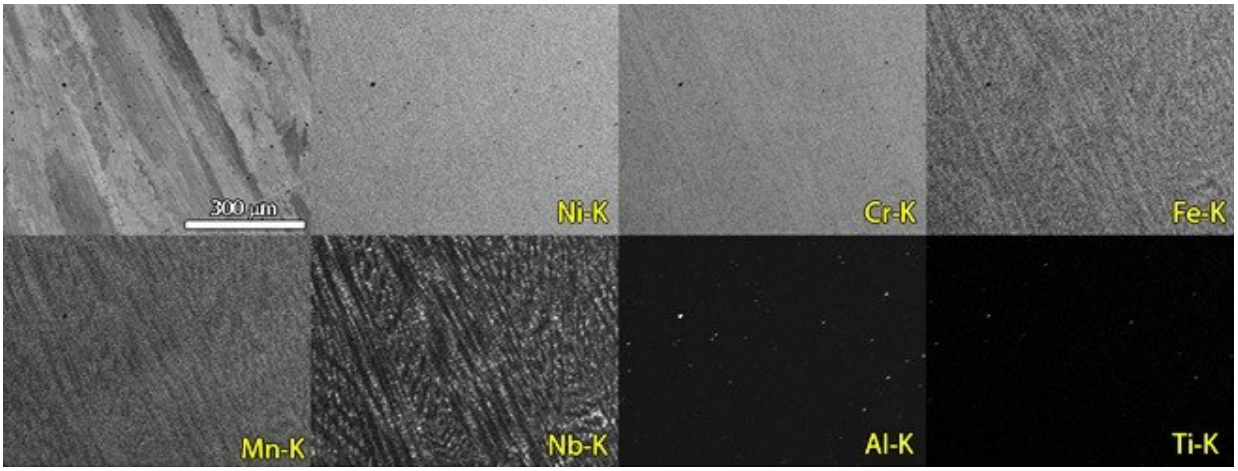

Figure 6. Low magnification SEM-EDS maps provide an overview of composition variations in the ANL alloy 152 v2 weldment. SEM-BSE image in the upper left shows the grain and dendrite structure.

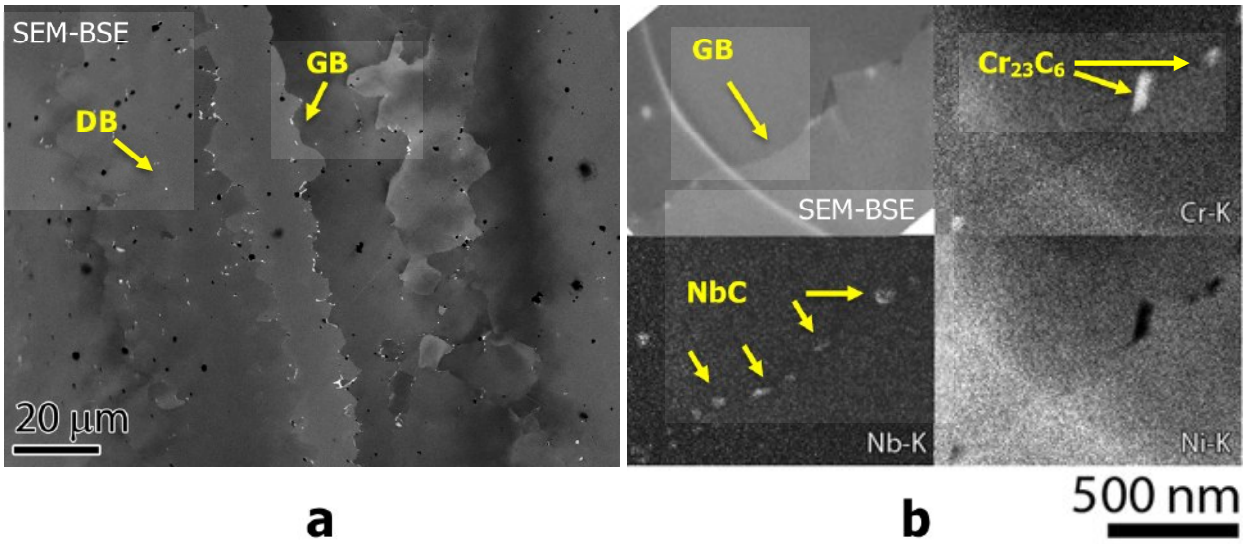

Figure 7. a) SEM-BSE image where heavier elements produce higher brightness. Bright precipitates decorating grain boundaries (GB) and dendrite boundaries (DB) are NbC. Black dot contrast is polishing debris. b) Higher magnification SEM-BSE and EDS images showing NbC and $Cr_{23}C_6$ carbides decorating a grain boundary.

Disclaimer: The work reported in this paper was supported by the Office of Nuclear Regulatory Research, U.S. Nuclear Regulatory Commission. The views expressed in this paper are not necessary those of the U.S. Nuclear Regulatory Commission.

Stress corrosion crack growth tests were performed on 0.5T compact tension (CT) specimens with the orientation of the two specimens relative to the weld slices shown in Figure 8. Care was taken to position the geometric crack plane of each specimen parallel to the long axis of the weld grain boundaries because this was perceived to be the most susceptible crack path. The first specimen (CT049) was oriented to assess the SCC susceptibility of the third layer of weld passes from the alloy 152 butter on the LAS, while the second specimen (CT080) was positioned to assess the second layer of weld passes from the butter. The notch and precrack were positioned so that SCC evaluations would be made on weld pass regions of higher hardness (220-260 kg/mm^2 as shown in Figure 4. Detailed three-dimensional EBSD characterization of the grain structure was performed on specimen CT049 after testing. These results are shown here in Figure 9 and Figure 10. These images reveal that the grains have an overall acicular shape with an aspect ratio of roughly 5:1. The Test Plane A images in Figure 10 show ~200 µm size grains with complex grain boundary shapes while the other images indicate that the long grain dimensions range from ~500 µm to 2000+ µm. Many grains have been observed to run continuously from one weld pass to a neighboring weld pass. This combination of relatively large grains and complex grain shape is thought to represent a very tortuous IG cracking mode that is not easily maintained.

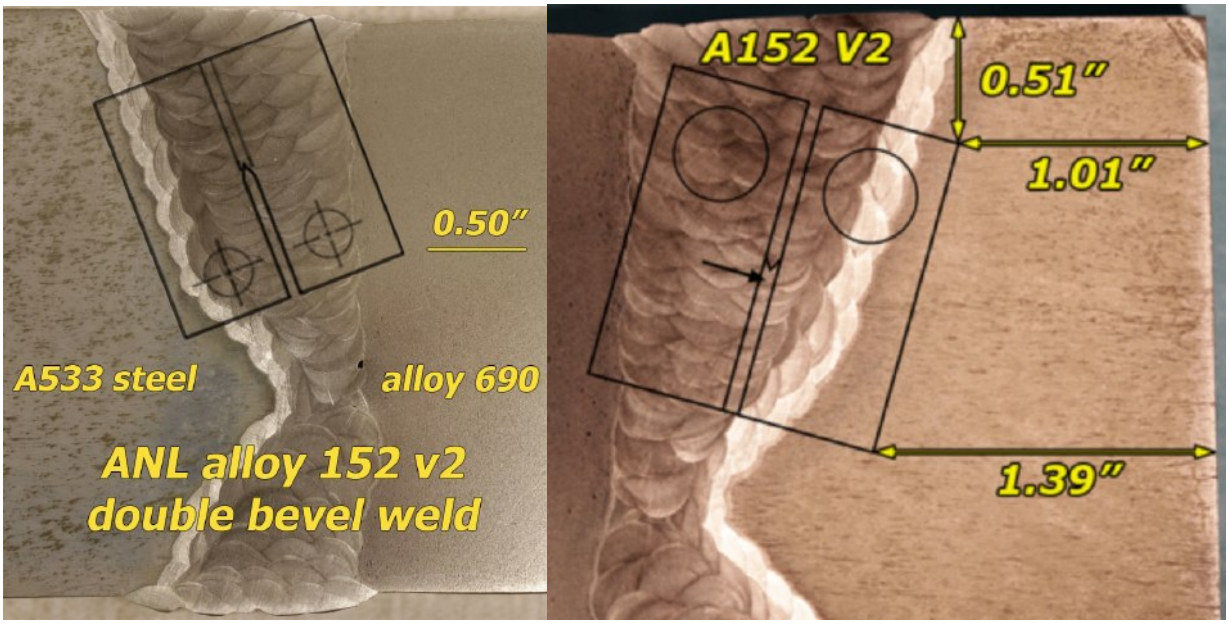

Figure 8. Locations of the 0.5T CT specimens extracted from two different slices of the alloy 152 v2 weldment. Image on the left is for the first test (CT049), while the image on the right is for the second test (CT080). Both specimens were oriented to align the elongated grain boundaries with the geometric crack path and within a region of higher hardness indicated in Figure 4.

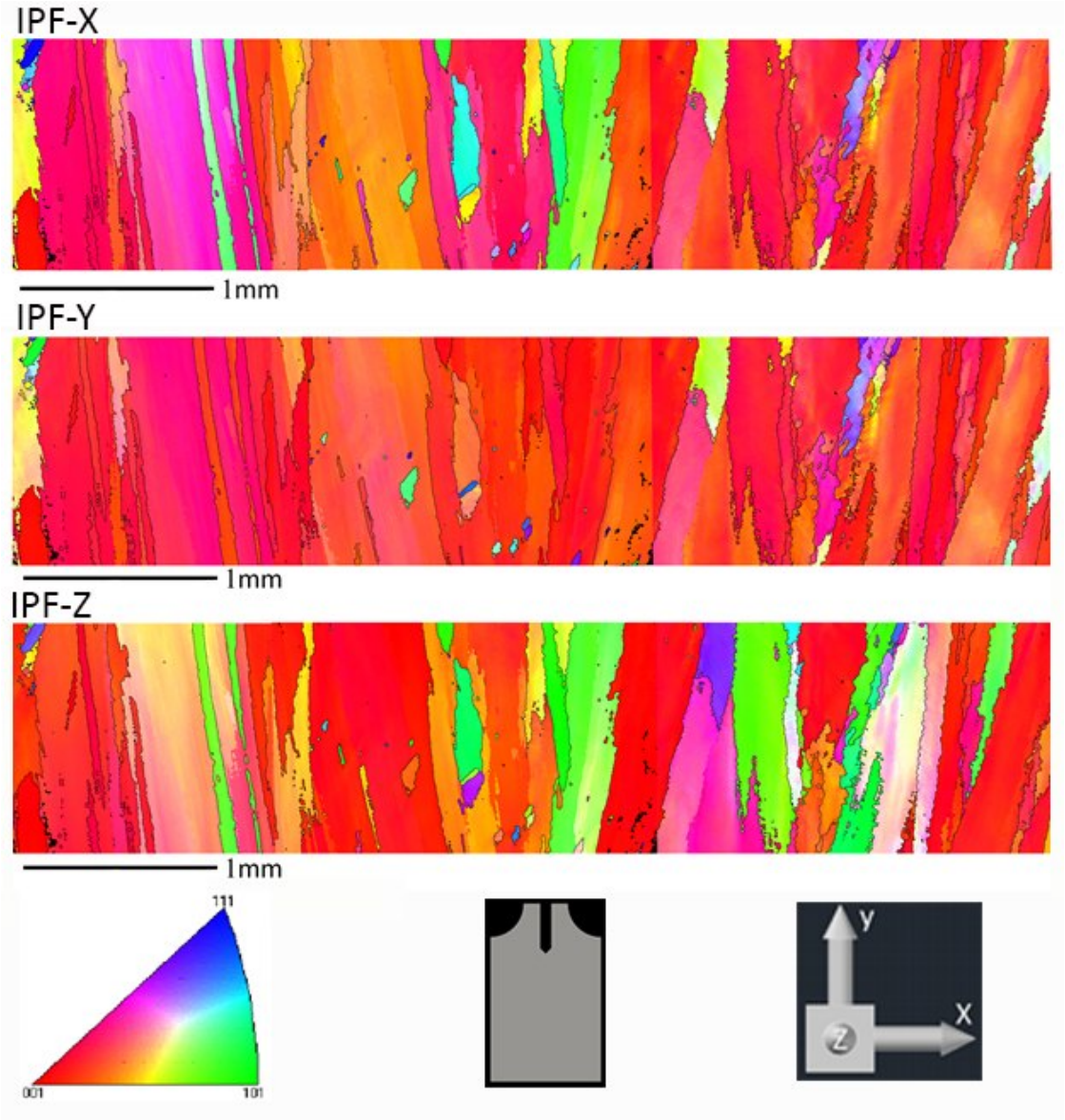

Figure 9. EBSD inverse pole figures illustrating the grain structure in the alloy 152 v2 CT049 CT specimen as viewed from the face of the specimen.

Disclaimer: The work reported in this paper was supported by the Office of Nuclear Regulatory Research, U.S. Nuclear Regulatory Commission. The views expressed in this paper are not necessary those of the U.S. Nuclear Regulatory Commission.

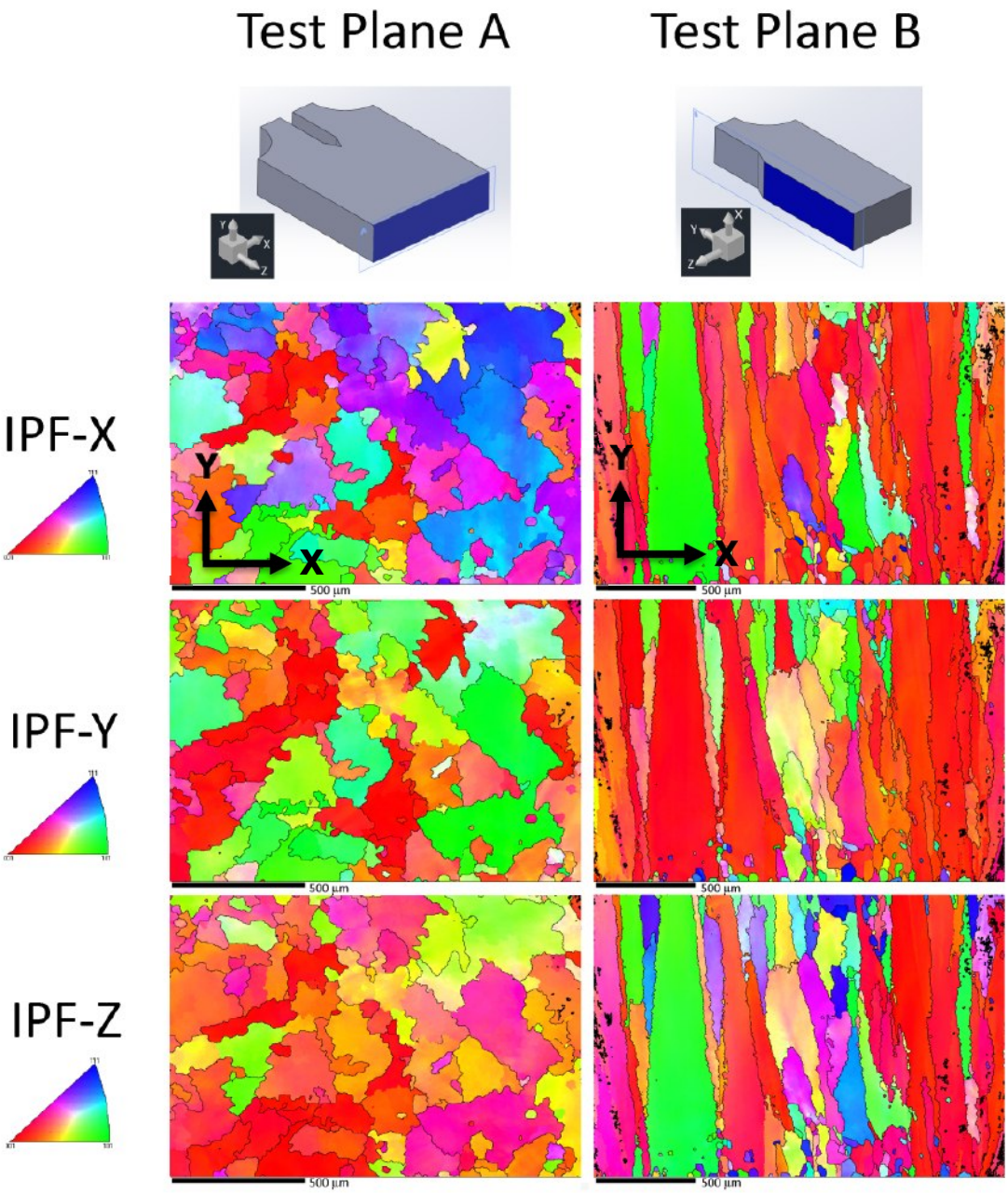

Figure 10. EBSD inverse pole figures illustrating the 3D grain structure in the alloy 152 v2 CT049 CT specimen as viewed from the end of the specimen (Test Plane A) or on the geometric crack plane (Test Plane B). The Z-axis is normal to the face of the specimen.

After specimen fabrication, the specimen side grooves were polished and etched to indicate the level of success in specimen positioning within the weldment and also to give an idea of the microstructure sampled during SCC testing. Images of the side grooves for the two specimens are shown in Figure 11 (CT049) and Figure 12 (CT080). In both cases, the specimens appear to be well aligned with the grain boundaries.

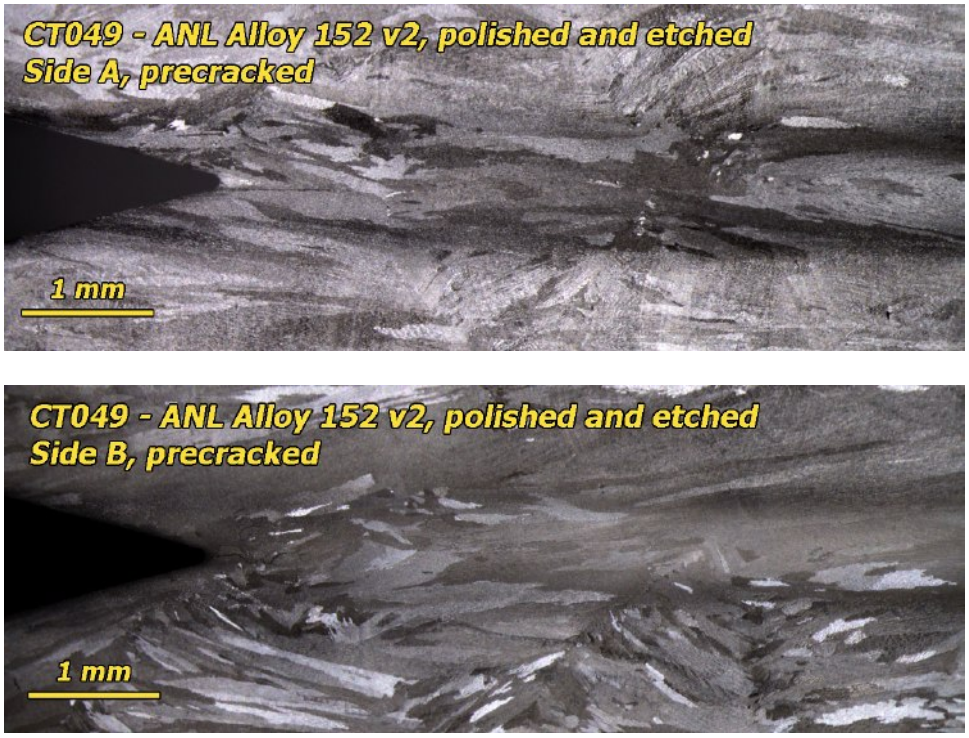

Figure 11. Optical images of the polished and etched side grooves for the first specimen (CT049) cut from the alloy 152 v2 weldment. Grain shape is highly variable, but based on these side-groove observations, the geometric crack path is well aligned with the grain boundaries of the elongated grains.

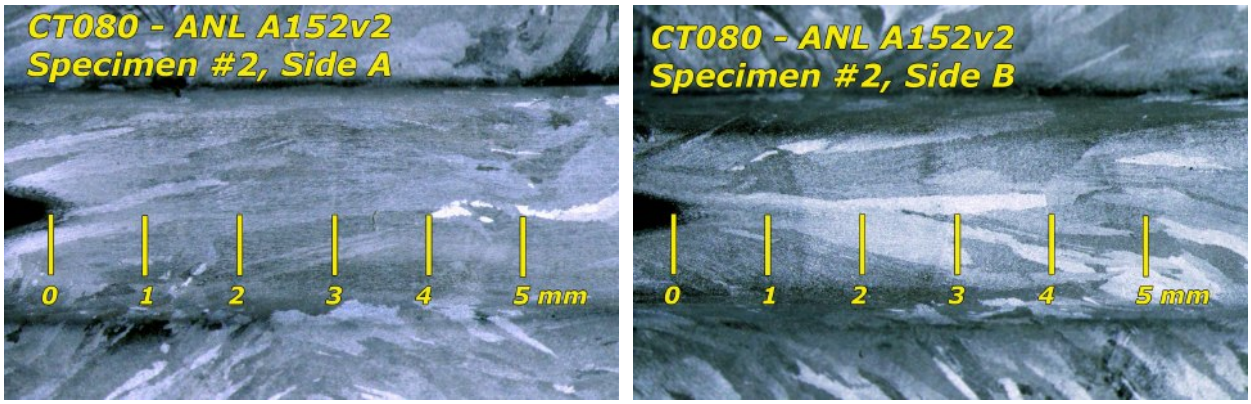

Figure 12. Optical image of the polished and etched side grooves for the first specimen (CT080) cut from the alloy 152 v2 weldment. Grain shape is highly variable, but based on these side-groove observations, the geometric crack path is well aligned with the grain boundaries of the elongated grains.

Disclaimer: The work reported in this paper was supported by the Office of Nuclear Regulatory Research, U.S. Nuclear Regulatory Commission. The views expressed in this paper are not necessary those of the U.S. Nuclear Regulatory Commission.

Test Setup and SCC Testing Approach

General performance aspects of the crack growth test systems are described in a previous paper **[9]**. Testing was performed at either 360°C or 320°C in simulated PWR primary water with 1000 ppm of boron and 2 ppm of lithium. The corrosion potential was held either at the Ni/NiO line (25 cc/kg H_2 at 360°C) or within the nickel metal stable regime (29 cc/kg H_2 at 320°C), while the standard target stress intensity (K) value was 30 MPa√m. Slight underestimation of the actual crack length by in-situ direct current potential drop (DCPD) occurred in the first test resulting in the actual K value drifting upward in a test. All data shown are corrected for observed final crack length and actual K values are noted in the crack growth rate (CGR) plots.

Specimens were precracked in air followed by further extension in the high-temperature water environment. After precracking, a variety of loading conditions were used to attempt to transition the TG crack front to an IGSCC crack. The general approach was to transition by going to slower and slower crack tip strain rates, typically by reducing the load cycling frequency. A range of R values (0.35-0.5) with either a symmetric or a sawtooth (e.g., rapid unload and slow reload) waveform were used and sometimes combined a hold time (1-24 h). The general philosophy was to choose "gentle" cycling and cycle + hold conditions that move the crack forward fast enough to encounter as many grain boundaries as possible while still allowing IG propagation if that is a favored path. For these tests, the most common final transitioning step before establishing constant K was a 980s/20s sawtooth cycle at R=0.5 with a hold time of 2.5 h. If propagation rates during the final transitioning steps were low (indicating limited SCC engagement across the crack front), additional cyclic and cycle + hold loading steps were often applied before going to constant K.

From a testing perspective, several factors make determination of the IGSCC susceptibility of weldments particularly challenging. The first factor is that a relatively large amount of crack extension is required during transitioning to effectively sample the grain boundaries of the very large and elongated grains in these materials. A second factor is that these high-Cr welds appear to be resistant to IG growth in PWR primary water. This leads to a simultaneous need for aggressive cycling to sample grain boundaries in a reasonable time and gentle cycling to provide the best conditions for IG engagement. Our approach to dealing with these opposing requirements has been to frequently retransition and maintain gentle cycling conditions for long times. Another issue is that ligaments or contacts can form in these weld metals even when aggressive cycling is used during transitioning sequences. Not only can crack growth sometimes be slowed in the vicinity of these ligaments, but ligaments also affect the DCPD-based measurement of crack extension. The effect of ligament or contact formation during constant K crack growth can be assessed by observing the immediate crack growth response during cycling after constant K exposures. Ligaments or contacts that break will produce an initially high crack growth rate for the given loading condition.

Results and Discussion

PWSCC Testing of Alloy 152 v2 Weld Specimen #1 (CT049)

An overview of the entire SCC test curve is shown in Figure 13. This test was conducted in 360°C primary water with a target K of 30 MPa√m, and five constant K evaluations were performed. DCPD underestimated the actual crack length in this test resulting in actual K values that were up to 30% higher than the target value. The approach to this test was to evaluate SCC response in five separated microstructural regions. In each transitioning sequence, a different set of transitioning conditions (cyclic and cycle + hold loading) was used to attempt to promote IG engagement along crack front prior to converting the test to constant K. The degree of IG engagement was determined from optical and SEM images of the crack growth surface after the test was completed (shown later), and the estimated percent engagement values are reported in Figure 13 where it can be compared to the crack position.

Approximately 50% IG engagement was achieved at the onset of gentle cycling (estimated to be at 0.001 Hz) during the first transitioning sequence and was maintained over ~0.5 mm of crack extension during the first and second transitioning sequences. More aggressive cyclic loading conditions at the onset of the third transitioning sequence (at 2500 h) reduced engagement to ~20% IG, and this fraction increased during the fourth and fifth transitioning sequences to ~60%. The transitioning approaches for CT049 can be roughly grouped into two categories. Transitioning sequences #1-4 attempted to produce IG engagement using cyclic loading frequencies of ~0.001 Hz (using rise/fall times of 500s/500s, 980s/20s, 600s/12s, or 1000s/12s) at R = 0.5 with the addition of hold times, while transitioning sequence #5 attempts to produce IG engagement through slower continuous cycling down to much lower frequencies (5000s/12s and 25000s/12s) but at a more aggressive R value of 0.35. The highest amount of IG engagement (60%) was achieved in the final transitioning sequence where low frequency continuous cycling at an R of 0.35 was used, however as much as 50% IG engagement was measured where more typical frequencies of ~0.001 Hz (R = 0.5) were used.

Initial constant K CGRs can be grouped into two categories of either $<1x10^{-9}$ mm/s or $2\text{-}6x10^{-9}$ mm/s. Examples of these behaviors can be found in Figure 14 and Figure 15. All constant K CGRs eventually dropped to $<1x10^{-9}$ mm/s. No clear correlation exists between constant K CGRs and the degree of IG engagement with very little (if any) SCC growth observed during the final constant K exposure (Figure 15). Response for the five SCC evaluations is summarized in Table 2. The possibility that contacts behind the crack front or fingered crack advance were masking the DCPD measurement during constant K testing was often assessed by applying gentle cyclic loading after constant K. In cases of significant masking of DCPD response during constant K, gentle cycling will immediately produce a CGR that is temporarily an order of magnitude higher than expected rates. Testing of the ANL 152 v2 material showed no such response with CGRs immediately matching the expected values, thus reinforcing the notion that little or no crack advance occurred during constant K.

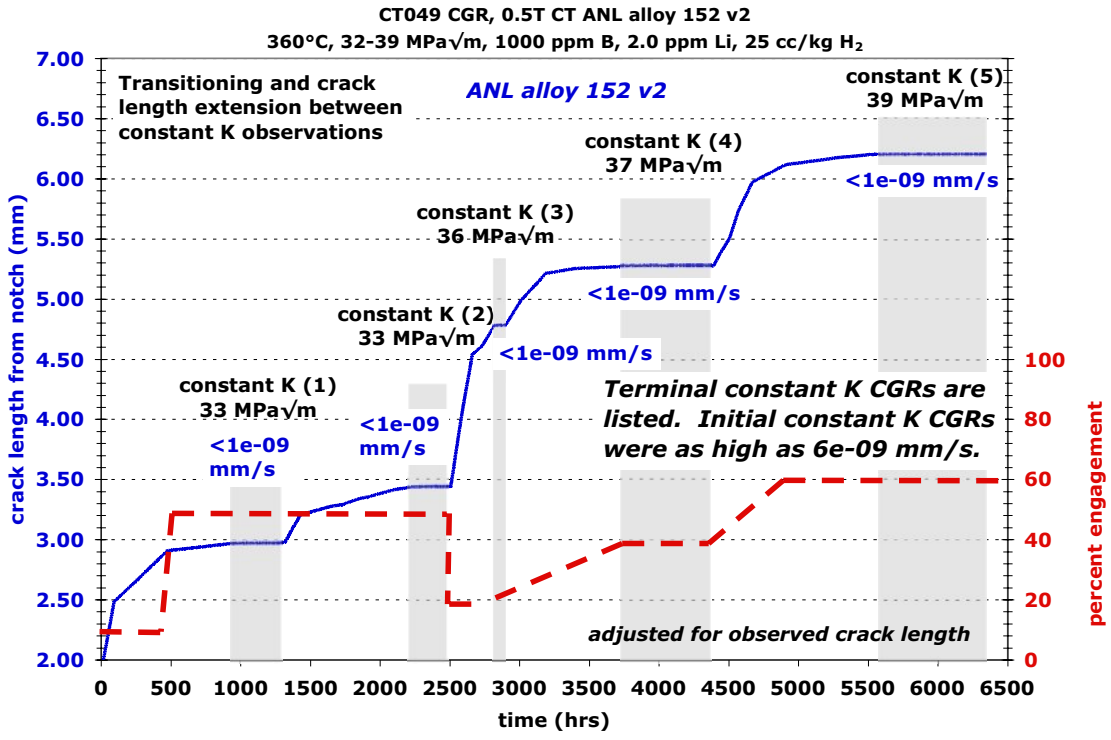

Figure 13. Overview of the entire test of the first alloy 152v2 weld specimen (CT049) performed in 360°C simulated PWR primary water. Dashed red line indicates the percent IG engagement.

Disclaimer: The work reported in this paper was supported by the Office of Nuclear Regulatory Research, U.S. Nuclear Regulatory Commission. The views expressed in this paper are not necessary those of the U.S. Nuclear Regulatory Commission.

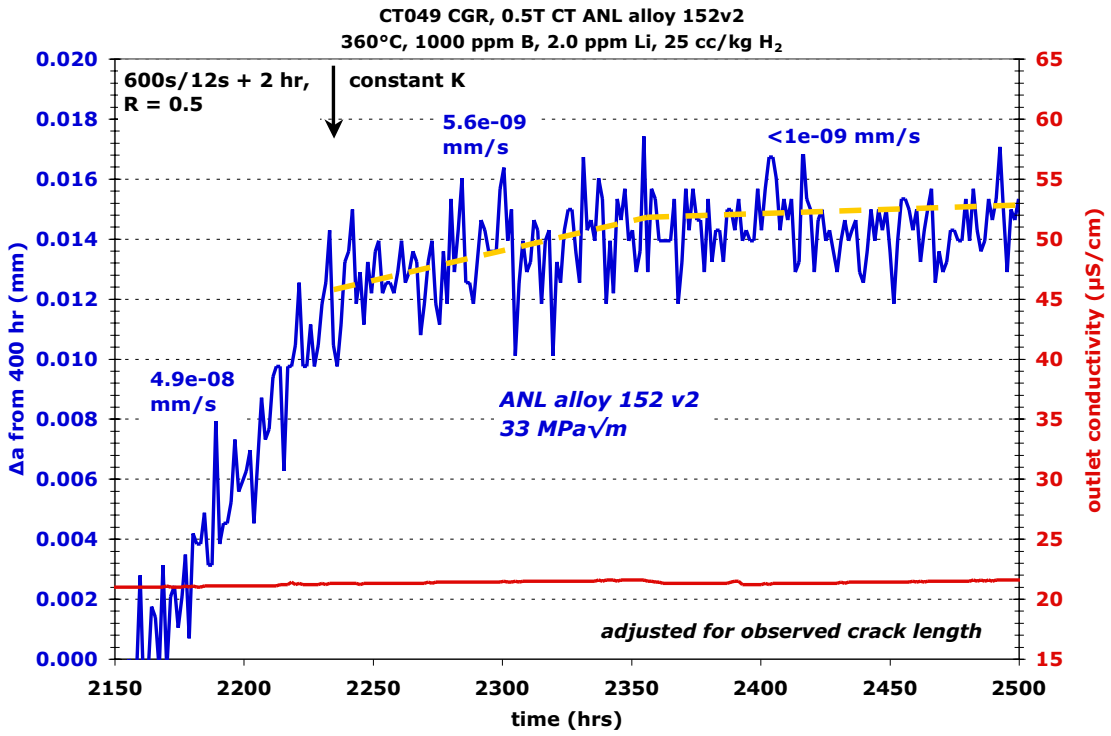

Figure 14. Crack growth response during the second constant K evaluation of CT049 in 360°C simulated PWR primary water. Stress intensity was ~33 MPa√m.

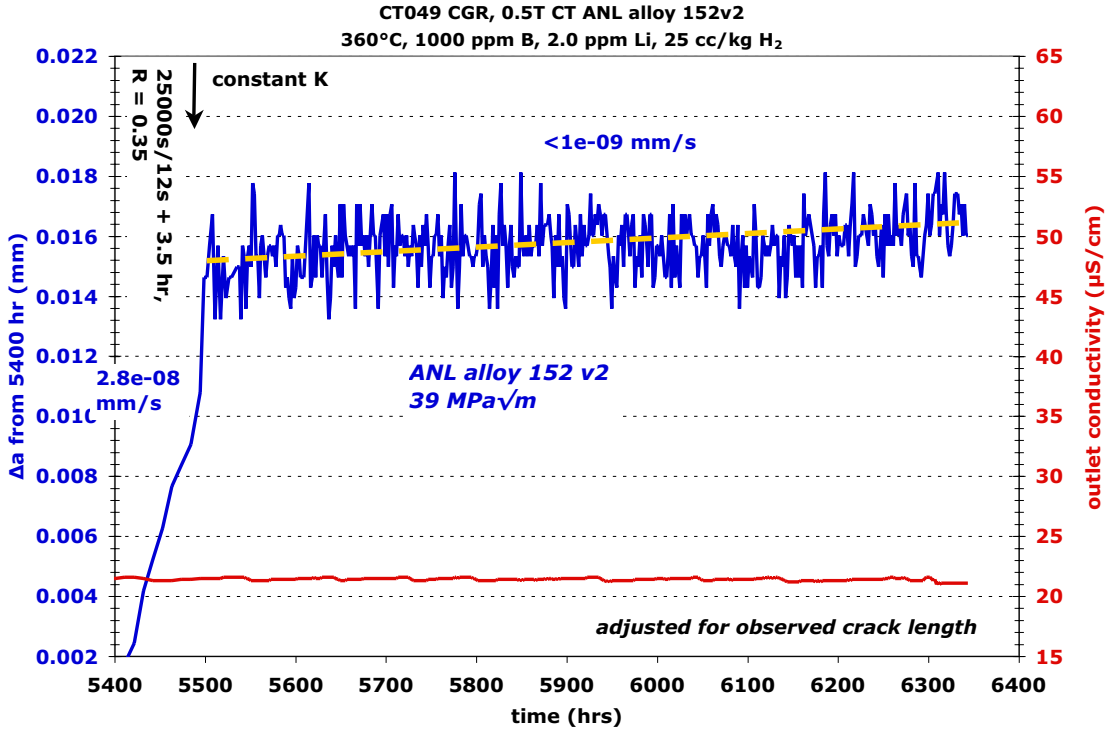

Figure 15. Measured crack-growth response during the fifth and final constant K evaluation of CT049 in 360°C simulated PWR primary water. Stress intensity was ~39 MPa√m.

Table 2. Summary of measured constant K CGRs for the CT049 specimen.

Trans. Sequence	Stress Intensity (MPa√m)	% IG	Initial Const K CGR (mm/s)	Final Const K CGR (mm/s)
1	33	~50	2.8×10^{-9}	$<1 \times 10^{-9}$
2	33	~50	5.6×10^{-9}	$<1 \times 10^{-9}$
3	36	~20	$<1 \times 10^{-9}$	$<1 \times 10^{-9}$
4	37	~40	2.2×10^{-9}	$<1 \times 10^{-9}$
5	39	~60	$<1 \times 10^{-9}$	$<1 \times 10^{-9}$

After SCC testing, the specimen was first sliced into an 8-mm thick piece and a 4-mm thick piece. The thicker piece was fatigued open for crack growth surface examinations, while the thinner piece was used for crack profile examinations. An optical image of the crack surface from the thicker piece is shown in Figure 16. Yellow lines were drawn where distinct changes in crack surface appearance were observed. In this optical image, areas of higher IG engagement have a rougher appearance than TG regions. IG cracking is responsible for the protrusions along the final crack front.

Detailed mapping of the IG/TG cracking morphology was performed using SEM imaging. SEM secondary electron (SE) images of regions within the four blue boxes in Figure 16 are shown in Figure 17. Significant amounts of IG cracking are present. The crenulated appearance clearly distinguishes IG from TG cracking (see also Figure 18). Comparison of such images to the optical images permitted measurement of the degree of IG engagement throughout the test, however, additional efforts were put into analysis of the final ~1.5 mm of crack extension by analyzing SEM-BSE and SE montages across the width of the surface as shown in Figure 19.

Observations of the crack profile from the 4-mm-wide piece of CT049 are shown in Figure 20 and Figure 21. In Figure 20, the air precrack can be clearly distinguished from the in-situ portion of the test. In this crack profile slice, the crack was entirely TG until the last ~1.4 mm, where it encountered and remained on a grain boundary. EBSD imaging shows that it is a high-angle grain boundary. The small branch cracks that formed near the final crack front are likely due to stresses driving the crack back down towards the geometric crack growth plane of the specimen. The final ~150 nm of IG crack extension shows nothing compositionally unique from SEM-EDS examinations (Figure 21). Major and minor elemental constituents appear compositionally similar to neighboring interdendritic boundaries. More detailed SEM and transmission electron microscopy (TEM) examinations are planned.

A key aspect of the crack growth morphology is very long sections of IG extension, often exceeding 1.5 mm. These long amounts of IG extension were probably made possible by having the geometric crack growth plane of the specimen well aligned to the long grain boundaries of the weld metal microstructure. IG extensions of this length clearly indicate that some grain boundaries in this weld are susceptible to environmental cracking under a variety of cyclic loading conditions. The loading conditions during the last 1.5 mm of testing ranged from constant K to somewhat aggressive cycling at 600s/12s (R = 0.5) and 1000s/12s (R = 0.35) showing that IG cracking will occur in this weld metal even under continuous cyclic loading. However, these observations also show that despite "easy" IG cracking along some grain boundaries, full IG engagement across the crack front was not achieved despite the application of a variety of gentle cyclic loading conditions over very long crack extensions. This suggests that grain shape and boundary orientation to the crack path play a significant role in IG propagation along with possible variations in grain boundary susceptibility.

Disclaimer: The work reported in this paper was supported by the Office of Nuclear Regulatory Research, U.S. Nuclear Regulatory Commission. The views expressed in this paper are not necessary those of the U.S. Nuclear Regulatory Commission.

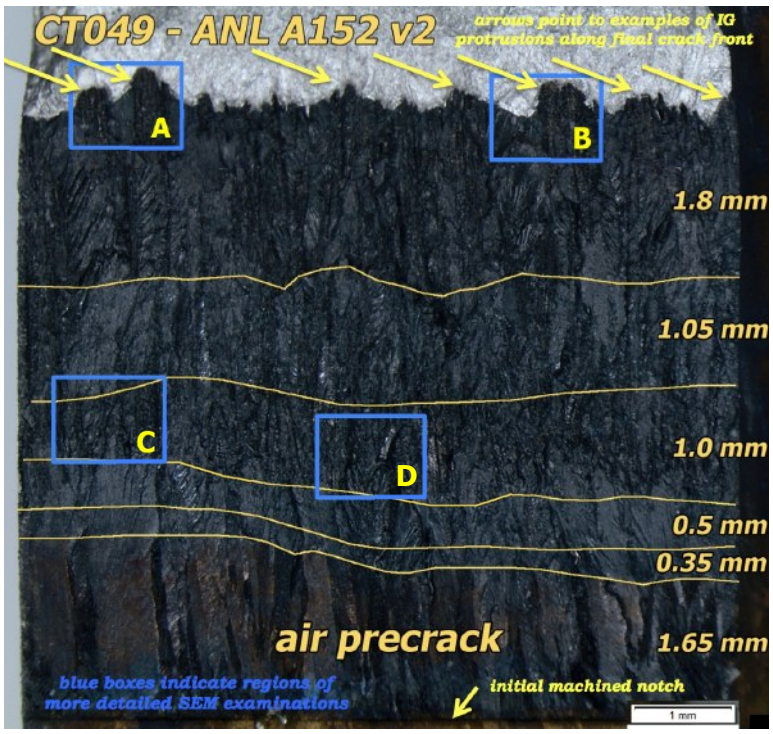

Figure 16. Crack-growth surface optical image of the 8 mm wide section of the CT049 specimen. Yellow arrows at top indicate examples of IG protrusions along the final crack front. Blue boxes indicate regions of higher resolution SEM examinations that are presented in Figure 17.

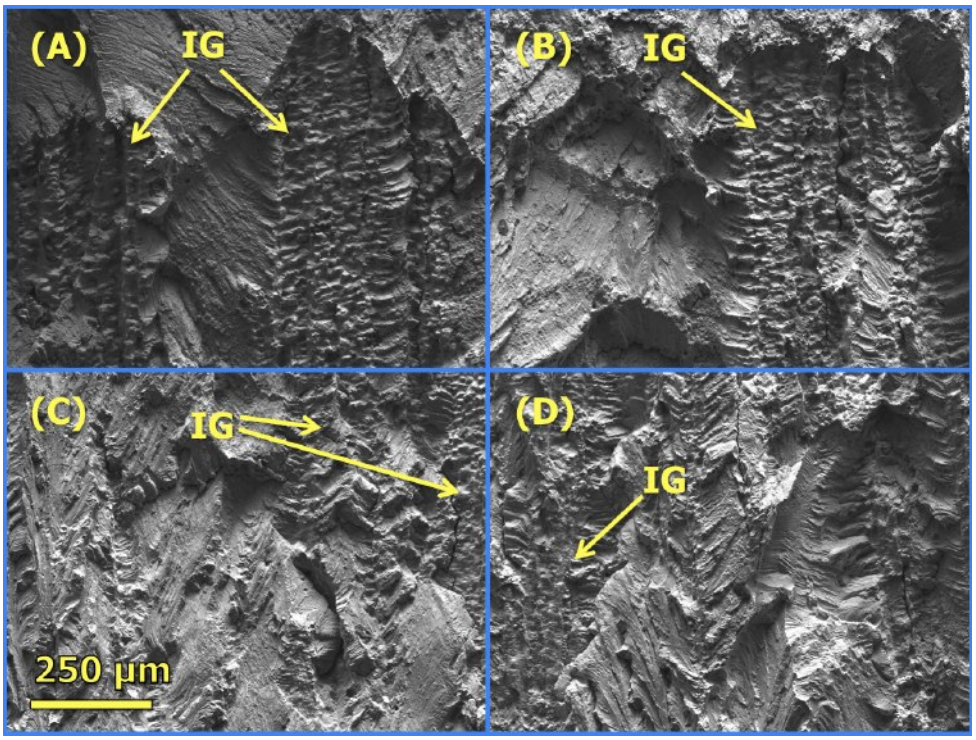

Figure 17. SEM-SE images of regions within the blue boxes in the optical image of the entire crack-growth surface for the CT049 specimen (Figure 16).

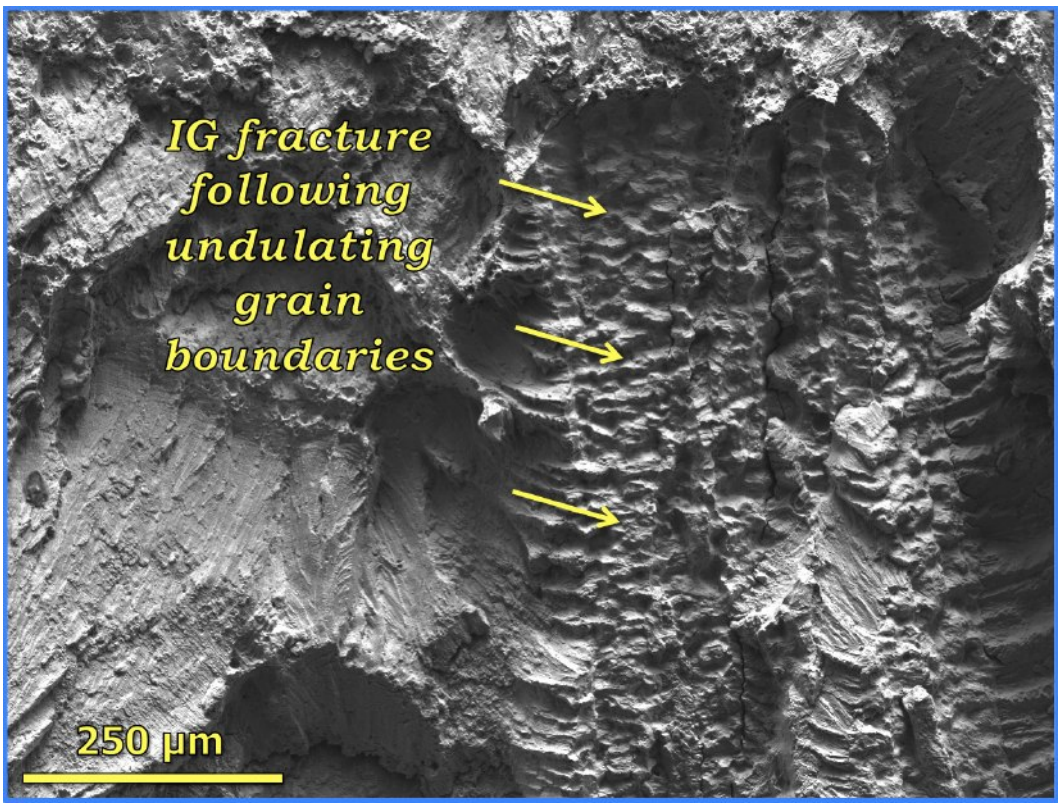

Figure 18. Higher magnification SEM-SE image illustrating the IG crack surface appearance in CT049.

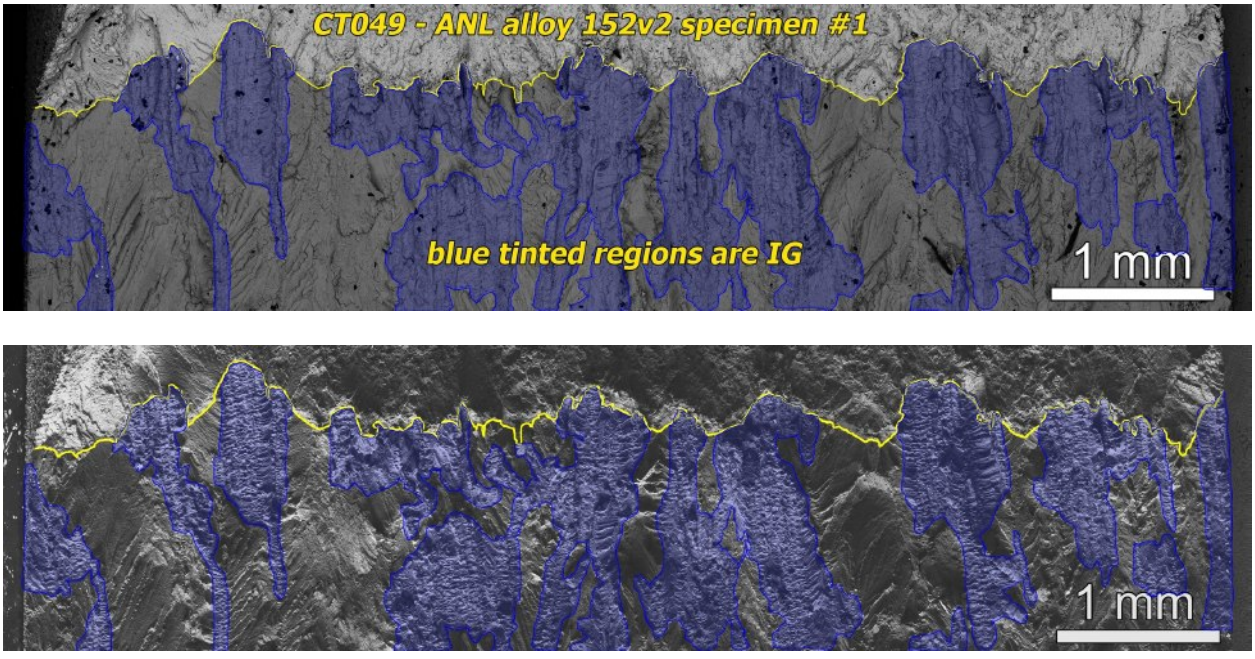

Figure 19. SEM-BSE (upper) and SE (lower) images showing IG regions (blue tint) along the final ~1.5 mm of the SCC test of CT049. Yellow line denotes the final crack front at the conclusion of the test.

Disclaimer: The work reported in this paper was supported by the Office of Nuclear Regulatory Research, U.S. Nuclear Regulatory Commission. The views expressed in this paper are not necessary those of the U.S. Nuclear Regulatory Commission.

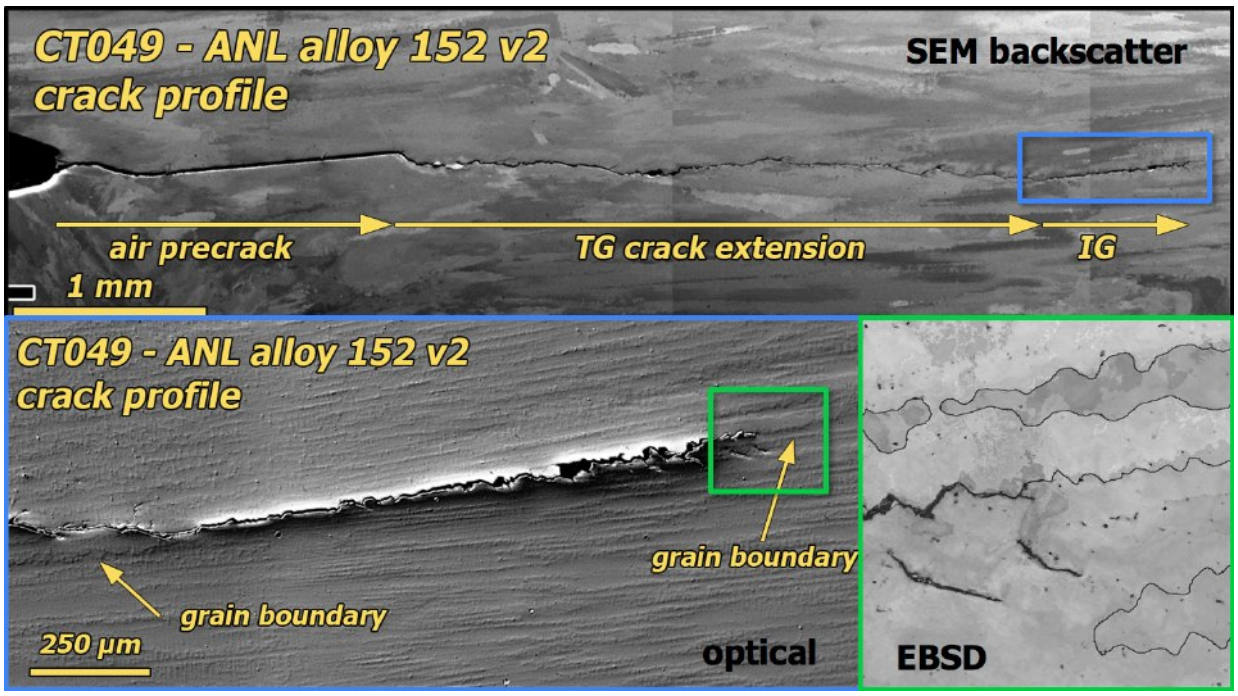

Figure 20. Compilation of SEM-BSE, optical, and EBSD images showing the crack path in profile from notch to final crack front in a side-surface cross section from the CT049 specimen.

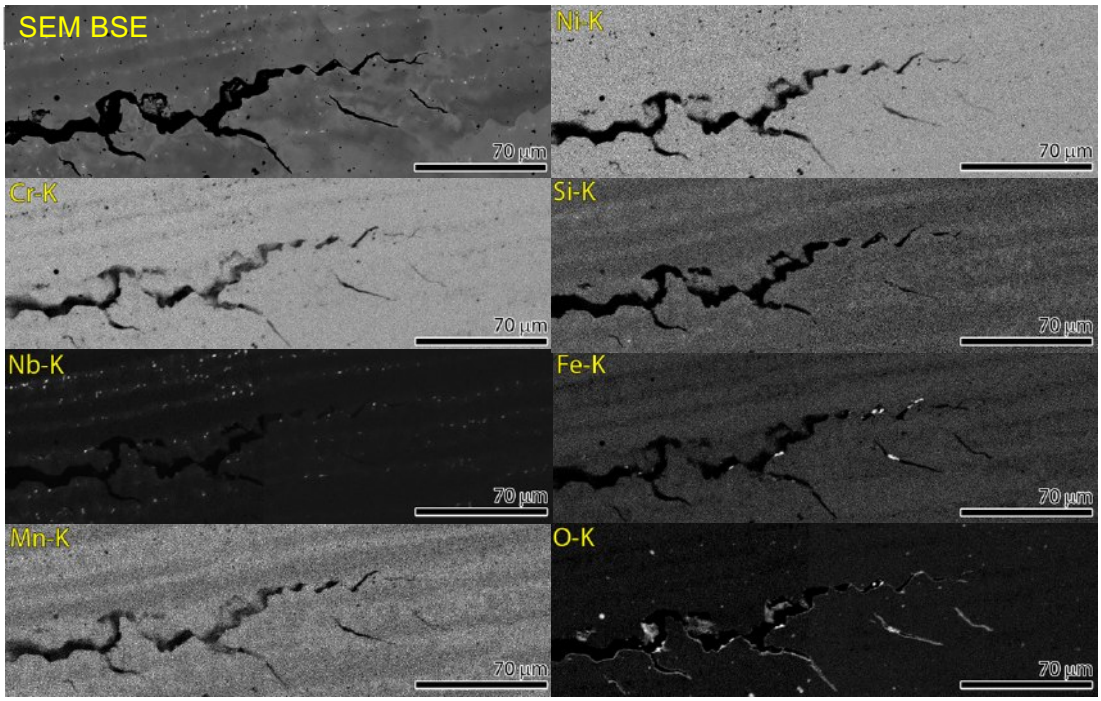

Figure 21. SEM-BSE and EDS maps showing elemental compositions along the final ~150 nm of the CT049 crack profile.

With such long amounts of IG extension occurring over a wide range of testing conditions, a major challenge in assessing the SCC response of this material is determining what amount of crack advance occurred during constant K loading. DCPD clearly shows crack advance during cyclic and cycle + hold loading, but DCPD indicates very little (few μm) or no growth during constant K testing. The crack surface of this specimen contains extensive IG cracking and localized IG protrusions at the final crack front. At this point in time, a method to factually isolate IG growth that occurs during constant K loading from that which occurs during cyclic or cycle + hold loading has not been determined. On the possibility that some IGSCC is occurring during constant K that DCPD did not accurately capture, constant K CGRs were estimated from the IG protrusions along the final crack front. For this analysis, it was assumed that constant K IG extension is that which occurred beyond TG tearing on either side of the IG cracking. This is illustrated in Figure 22 for two extreme examples (these are two of the same images in Figure 17) where the white dashed line indicates the postulated start of constant K IG growth, and the white arrows indicate the maximum extension. Following this method on all the protrusions along the final crack front in Figure 16, engaged constant K CGRs were calculated to be as high as ~$1x10^{-7}$ mm/s, however the majority of the measurements gave measurements closer to 1-$2x10^{-8}$ mm/s.

It is important to recognize that while this analysis of the final crack front gives average constant K CGRs in the engaged regions of ~1-$3x10^{-8}$ mm/s, the shape of the final crack front shows no indication of a tendency for the crack to become progressively more IG during constant K loading. The only constant K IG cracking that may have occurred was from regions that were already engaged prior to setting the test to constant K. In addition, the morphology of the engaged regions of the final crack front shows no indication of IG expansion or ballooning. Instead, the IG regions typically have a pointed shape suggesting that the degree of IG engagement was decreasing as time progressed. The same resistance to achieving very high degrees of IG engagement was also observed during crack transitioning. While 60% engagement is higher than any other alloy 152/52 weld metal specimen tested by the authors, there is no indication that full engagement would have been achieved if the transitioning had continued for much longer periods of time. The torturous grain boundary shape of this material favors this assessment that only limited engagement is likely.

The inability to obtain >60% IG engagement during transitioning or obtain an increase in IG cracking during constant K loading is somewhat in contrast to the ease at which portions of the specimen transitioned to (and maintained) IG growth for several millimeters at mildly aggressive fatigue cycling conditions with CGRs of more than $1x10^{-7}$ mm/s. The overall assessment of this specimen is that while significant IG engagement is clearly possible, widespread sustained IGSCC is not.

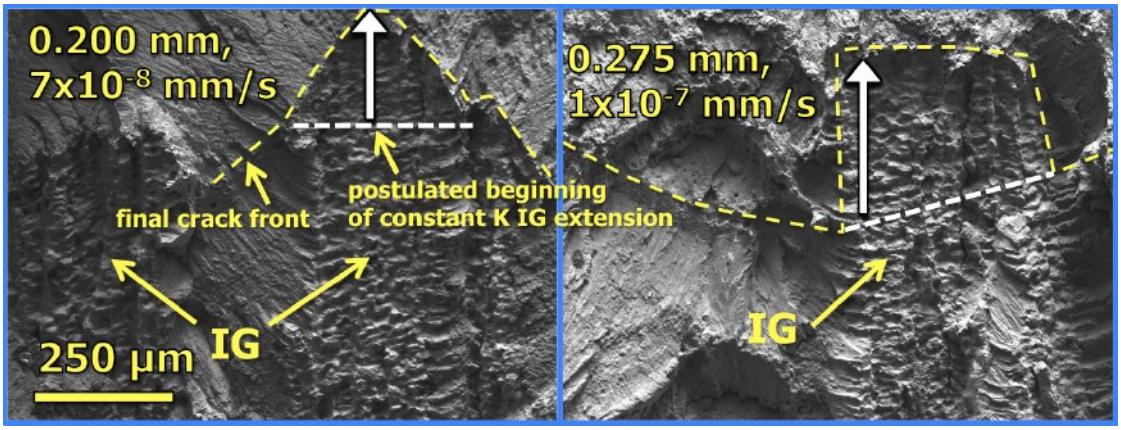

Figure 22. Illustration of postulated constant K IG extension along the final crack front of CT049.

Disclaimer: The work reported in this paper was supported by the Office of Nuclear Regulatory Research, U.S. Nuclear Regulatory Commission. The views expressed in this paper are not necessary those of the U.S. Nuclear Regulatory Commission.

PWSCC Testing of Alloy 152 v2 Weld Specimen #2 (CT080)

The observation of significant IG engagement but with apparent low CGRs in the CT049 specimen prompted the decision to run a second test on this weldment. As described in the experimental section, this specimen was located in a slightly different position. The CT080 specimen was also rotated 180 degrees relative to CT049 so that cracking would progress towards the weld root rather than towards the crown. As with the first specimen, this one was again aligned parallel to the grain boundaries as best as possible (Figure 12). An overview of the entire DCPD-based crack growth response is shown in Figure 23. The first portion of the test was conducted under the same environmental conditions as the prior CT049 test (360°C at the Ni/NiO oxide stability). Similar transitioning techniques were also applied in this first part of this test, i.e., progressively more gentle cycling leading to gentle cycle + hold loading before assessing constant K response. The first constant K assessment that was started at ~1950 h produced very low crack growth rates of $<1x10^{-9}$ mm/s as shown in Figure 24. After ~600 h at constant K, gentle cyclic loading was applied and produced typical CGRs for this loading condition, indicating that DCPD had not been masked by contact formation or fingered crack advance during constant K. The crack was then aggressively advanced to a new region where retransitioning steps were started. Crack growth rates during these transitioning steps were found to be identical to earlier in the test and similar to that in the prior test (CT049).

Having duplicated the crack-growth response during transitioning and constant K of the first test (360°C) based on in-situ DCPD, the environmental conditions and crack transitioning methods were altered to approximate those used by ANL on the two alloy 152 welds using the WC04F6 weld filler metal **[5-7]**. Thus, test temperature was reduced to 320°C and the dissolved hydrogen concentration shifted to 29 cc/kg in the Ni-metal stability regime. Common ANL transitioning methods use progressively more gentle cyclic loading steps and hold times just like PNNL and many other SCC testing laboratories, however the particular cyclic waveforms are slightly different. ANL tends to favor a 600s/12s (R = 0.5) load cycle for their most gentle continuous cyclic loading condition for this material and test temperature, and the most common hold time is 2 hours. As part of their crack-growth assessment, ANL also occasionally uses a periodic partial unloading step that consists of a 12s/12s (R = 0.5) load cycle every 1 or 2 hours. Since in-situ constant K correction is not done at ANL, this feature was turned off as well, and K was allowed to increase with crack length and SCC was evaluated under constant load conditions. Lastly, ANL assesses CGR response during transitioning by comparing the in-situ environmental CGR to a calculated air CGR that is an empirical fit to air fatigue tests on alloy 600, 182, and 690 **[7,10]**. Inputs into the air fatigue formula include stress intensity, load ratio and temperature. The ratio of the environment CGR to the calculated air fatigue CGR (env/air ratio) is used as a gauge for estimating the SCC engagement during transitioning. All these aspects of SCC testing were adopted for the second half of this test.

During testing at 320°C, the CGR at 600s/12s (R = 0.5) cycling was frequently measured as suggested by the many small ramps in 320°C portion of the overview test plot (Figure 23). The env/air CGR ratio consistently hovered between 2-3 for 600s/12s continuous cycling transitioning steps, and the addition of a hold time tended to increase this ratio by ~10%. The env/air CGR ratios for the first transitioning sequence at 320°C are shown in Figure 25, where they are compared to env/air ratios measured during the two transitioning sequences at 360°C. These ratios at the first 320°C transitioning sequence are typical of those in later transitioning sequences at 320°C, and they are similar or slightly lower than the values determined at 360°C. Constant load SCC evaluations were made three times at 320°C with all evaluations producing CGRs that quickly dropped below $1x10^{-9}$ mm/s, as illustrated by the last attempt shown in Figure 26. As with testing at 360°C, application of gentle cycling always showed no indication that DCPD was being masked during constant load exposures.

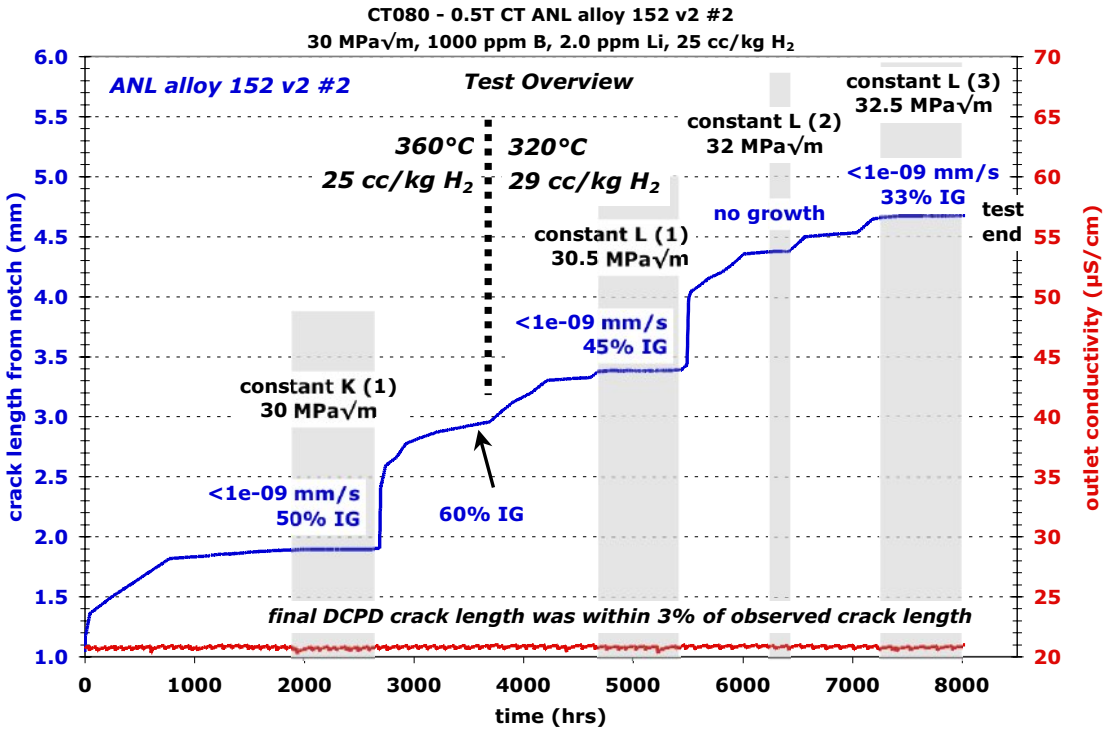

Figure 23. Overview of CGR test on the second alloy 152 v2 specimen (CT080) performed in 360°C (0-3800 hours) and 320°C (3800-8000 hours) simulated PWR primary water. Terminal constant K CGRs are listed.

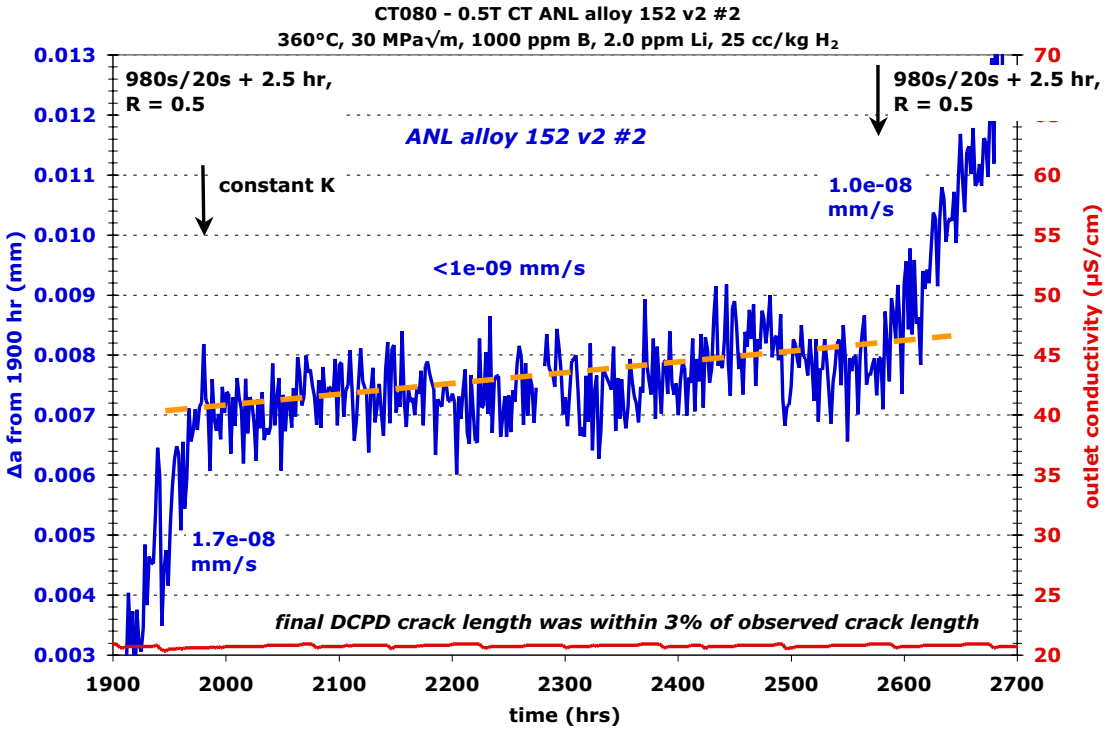

Figure 24. Constant K crack growth response following the first transitioning sequence on the alloy 152 v2 specimen CT080 in 360°C simulated PWR primary water.

Disclaimer: The work reported in this paper was supported by the Office of Nuclear Regulatory Research, U.S. Nuclear Regulatory Commission. The views expressed in this paper are not necessary those of the U.S. Nuclear Regulatory Commission.

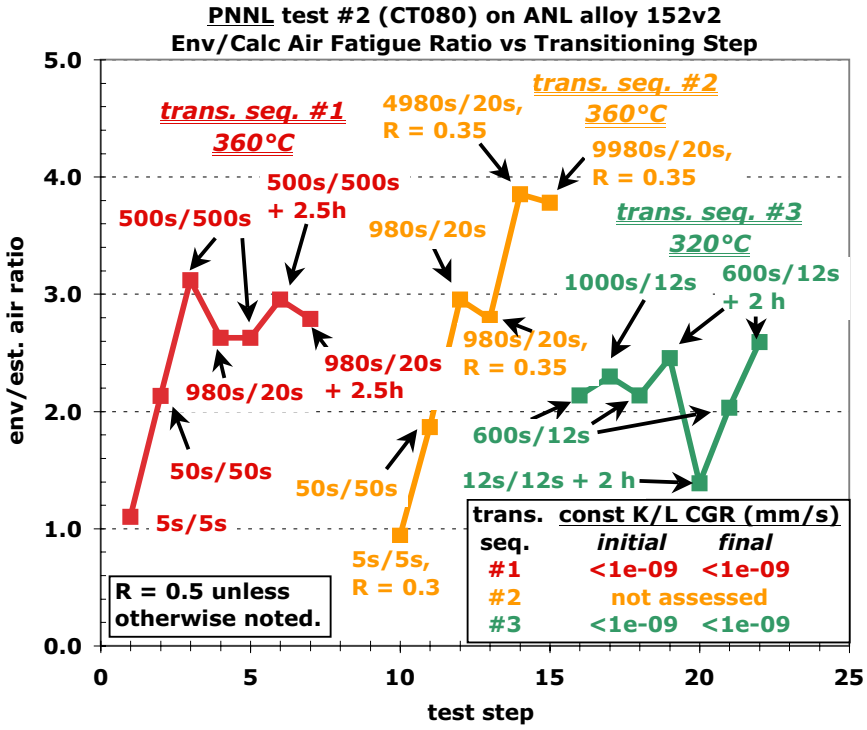

Figure 25. Env/air ratio during the first three transitioning sequences (two at 360°C and one at 320°C) for the second test on the alloy 152 v2 weldment (CT080).

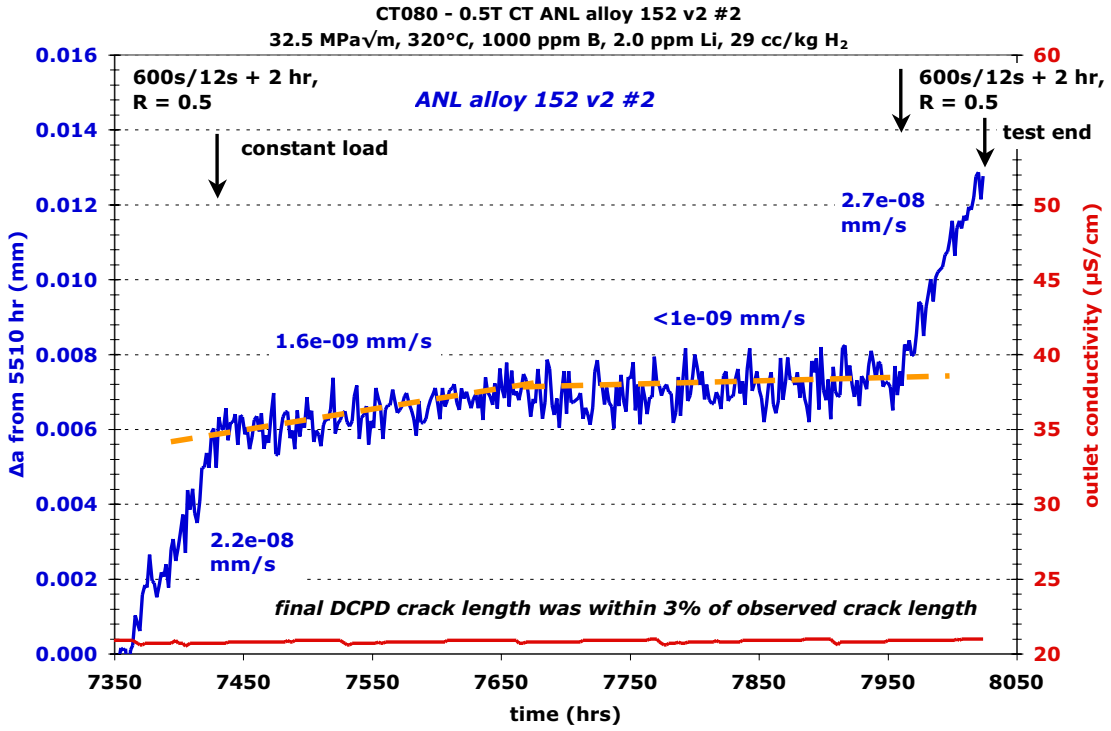

Figure 26. Third constant load observation on the alloy 152 v2 specimen CT080. This portion of the test was conducted in 320°C simulated PWR primary water.

Post-test examinations were conducted in a similar fashion to the prior test on the CT049 specimen. The CT080 specimen was sectioned into an 8-mm-wide slice for crack-growth surface observations and a 4-mm-wide slice for crack profile observations. Optical imaging of the crack-growth surface (Figure 27) revealed differing appearances for the portions of the test at 360°C and 320°C. The degree of IG engagement was examined in detail along the final crack front using SEM-BSE imaging as shown in Figure 28 where regions of IG cracking are highlighted in blue. Complimentary SEM-SE images were also taken to confirm crack morphologies. The degree of IG engagement along the final crack front was estimated to be ~33%. Assessment of the remainder of the surface using the optical image produced a value of ~45% during the first constant load assessment at 320°C, while 50-60% peak IG engagement was measured at 360°C, consistent with the first test on this weldment. The crack profile image in Figure 29 (left side of the specimen in Figure 27) was found to have primarily TG cracking for this cross-section location.

The general conclusion for the test on this second alloy 152 v2 specimen (CT080) is that similar response was seen at 360°C, i.e., 50-60% IG engagement and terminal constant K CGRs were $<1x10^{-9}$ mm/s. When the test temperature was lowered to 320°C, the degree of IG engagement decreased and constant load CGRs at 320°C were again $<1x10^{-9}$ mm/s.

Figure 27. Optical image of the 8-mm-wide section of the crack-growth surface of the second alloy 152 v2 specimen (CT080) tested in 360°C and 320°C simulated PWR primary water.

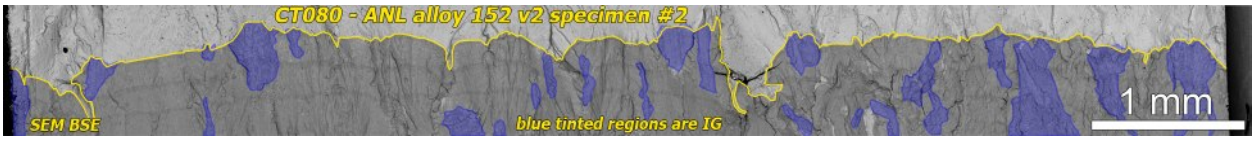

Figure 28. SEM BSE image of the final ~1 mm of crack growth of the second alloy 152 v2 specimen (CT080). This portion of the test was at 320°C.

Disclaimer: The work reported in this paper was supported by the Office of Nuclear Regulatory Research, U.S. Nuclear Regulatory Commission. The views expressed in this paper are not necessary those of the U.S. Nuclear Regulatory Commission.

Figure 29. Optical image of the side-surface cross section taken from the second alloy 152 v2 specimen (CT080) after SCC testing.

Comparison to Other Alloy 152/52 Weld Metals and Alloy 690

Following the same crack-surface examination methods, the degree of IG engagement and the estimated average CGR of the engaged regions for several alloy 152/52 specimens tested at PNNL were determined and compared to the alloy 152 v2 values (Table 3). The DCPD-based constant K (or constant load) CGRs are generally similar among the weldments with low CGR values between 0.5 and $5x10^{-9}$ mm/s. These CGRs for alloy 152/52 are consistent with the test results from many laboratories summarized in Figure 1. However, the maximum SCC rates are a factor of 2-4x lower than reported by ANL **[5-7]** on several tests on the alloy 152 welds made using the heat WC04F6 weld filler metal. The upper bound CGR on the PNNL tests, as indicated by the estimated engaged IG CGRs, are all largely similar at $1\text{-}3x10^{-8}$ mm/s. These maximum, local CGRs are comparable to the DCPD-based values reported by ANL. Finally, the degree of IG engagement was highest in the alloy 152 v2 weldment, suggesting that it may be more susceptible to IG cracking. ANL did report slightly higher IG engagement of up to ~70% engagement in their tests on the 152 v2 weldment **[7]**. The length of the IG engaged regions was not quantified in detail, but engaged regions of 1+ mm length were found on all but CT032 and CT043 (Table 3).

Comparison to alloy 690 is somewhat limited due to the differing microstructures, however the alloy 152 v2 can be compared using microhardness as a basis. As noted in the Experimental section, Vickers hardness of the alloy 152 v2 was ~200-260 kg/mm^2 in the regions that were SCC tested, while alloy 690TT, 17%CR alloy 690TT and 31%CR alloy 690TT tested at PNNL had average values of 175, 240 and 300 kg/mm^2, respectively. SCC testing of these alloy 690 materials at 350-360°C produced the following results **[11]**: The as-thermally treated material exhibited CGRs of $\leq 1x10^{-9}$ mm/s and showed no IG engagement. The 17% CR tested in the S-L orientation exhibited near-steady CGRs of $\sim 2.5x10^{-9}$ mm/s and showed ~5% engagement. Finally, the 31%CR tested in the S-L orientation exhibited steady CGRs of $\sim 1x10^{-7}$ mm/s and had ~100% IG engagement. The alloy 152 v2 has a hardness roughly between the non-CR and the 17% CR alloy 690, and its constant K/load CGRs are consistent with this comparative hardness. However, the high degree of engagement in the alloy 152 v2 is more consistent with the 31% CR alloy 690.

One possible conclusion that can be drawn from the current analysis is that if a very high degree of engagement is achieved, SCC CGRs of $1\text{-}3x10^{-8}$ mm/s may result in alloy 152/52 weldments. However, testing indicates that extensive transitioning efforts produce only partial IG engagement, and when converted to constant K/load conditions, little or no IGSCC occurs. The inability to clearly distinguish between IG cracking during transitioning and constant K/load test conditions makes the calculation of

engaged IGSCC CGRs questionable. What can be unambiguously determined from the crack-growth surface analysis is that there is no tendency for the degree of IG engagement to improve during constant K/load conditions. In fact, the most likely conclusions are that IGSCC growth either stalls at the onset of constant K/load, or the degree of IG engagement begins to slowly decrease and again SCC growth stalls. The wide range of possible interpretation of the results indicates that additional testing and analyses on alloy 152/52 welds are needed to better establish heat-to-heat variability in SCC susceptibility.

Table 3. Percent engagement, DCPD-measured CGRs, and calculated CGR of engaged IG protrusions of alloy 152/52 weldments tested at PNNL.

Material	Specimen ID	Test Temp. (°C)	% IG Engaged	DCPD-CGR Range (mm/s)	Est. Avg. CGR of IG Protrusions (mm/s)**
Alloy 152 v2 ANL	CT049	360	50-60	$0.5\text{-}1.8\times10^{-9}$	$\sim3\times10^{-8}$
Alloy 152 v2 ANL	CT080	360	50-60	$<1\times10^{-9}$	$\sim1\times10^{-8}$
Alloy 152 v2 ANL	CT080	320	33-45	$0.5\text{-}1.6\times10^{-9}$	$\sim1\times10^{-8}$
Alloy 152 MHI	CT013	325	25	0.3×10^{-9}	$\sim2\times10^{-8}$
Alloy 152 MHI	CT017, CT018	350	40	$0.3\text{-}1.7\times10^{-9}$	$\sim3\times10^{-8}$
Alloy 52 AREVA	CT024, CT032	350	10	$0.5\text{-}1.2\times10^{-9}$	$\sim2\times10^{-8}$
Alloy 52 MHI	CT025, CT033	350	10	$0.8\text{-}3.5\times10^{-9}$	$\sim3\times10^{-8}$
Alloy 52M VG KAPL	CT041	360	30	$3.8\text{-}4.6\times10^{-9}$	$\sim1\times10^{-8}$
Alloy 52M NG KAPL	CT040	360	5	$0.8\text{-}1.6\times10^{-9}$	$\sim2\times10^{-9}$
Alloy 52M NG+HC KAPL	CT042, CT043	360	5	$1.1\text{-}2.8\times10^{-9}$	$\sim2\times10^{-8}$
Alloy 52MSS Spec Metals	CT050	360	25	$0.5\text{-}0.9\times10^{-9}$	$\sim2\times10^{-8}$

**These CGRs are calculated based on the possibility that IG protrusions along the final crack front formed during constant K testing, however this appears unlikely.

Summary

CGR tests were conducted in simulated PWR primary water on an alloy 152 weldment that was found to be susceptible to SCC in testing at ANL. PNNL tests showed initial DCPD-based constant K or constant load CGRs were below 6×10^{-9} mm/s, and terminal CGRs were below 1×10^{-9} mm/s. Post-test examination revealed that continuous IG cracking for lengths of 1+ mm readily formed in the weld, but no more than 60% IG engagement was achieved across the specimens despite the use of a wide range of transitioning steps at many different microstructural regions. The long amounts of IG cracking clearly demonstrated that IG growth readily occurred at cyclic loading frequencies as low as ~0.05 Hz. However, it was not possible to determine if any portion of these IG regions continued to grow during constant K/load exposures. If the IG protrusions along the final crack front are assumed to form at constant K/load, then these protrusions would have had an average IGSCC CGR of $\sim3\times10^{-8}$ mm/s. It is important to note that the crack front morphology shows no indication of IG expansion during the constant K/load exposures, and instead points towards either immediate cessation of crack extension at the onset of constant K/load or eventual crack arrest. These observations indicate that this material is very resistant to SCC, although it appears to be less resistant than non-cold worked alloy 690 where IG engagement is virtually non-existent.

Disclaimer: The work reported in this paper was supported by the Office of Nuclear Regulatory Research, U.S. Nuclear Regulatory Commission. The views expressed in this paper are not necessary those of the U.S. Nuclear Regulatory Commission.

Acknowledgements

Primary support for this research is from the U.S. Nuclear Regulatory Commission. Helpful interactions with D. S. Dunn, B. Alexandreanu and P. L. Andresen are acknowledged along with the technical assistance of R. J. Seffens, A. D. Guzman and C. E. Chamberlin. Pacific Northwest National Laboratory is operated for the U.S. Department of Energy by Battelle Memorial Institute under Contract DE-AC06-76RLO 1830.

References

1. M. B. Toloczko and S. M. Bruemmer, "Crack Growth Response of Alloy 152 and 52 Weld Metals in Simulated PWR Primary Water", *Proc. 14th Int. Conf. Environmental Degradation of Materials in Nuclear Power Systems – Water Reactors,* Virginia Beach, VA, American Nuclear Society, 2009.

2. M. B. Toloczko, M. J. Olszta, S. M. Bruemmer, "Stress Corrosion Crack Growth of Alloy 52M in Simulated PWR Primary Water," *Proc. 15th Int. Conf. Environmental Degradation of Materials in Nuclear Power Systems – Water Reactors,* Colorado Springs, CO, The Metals Society, 2011.

3. P. L. Andresen, M. M. Morra, J. Hickling, A. Ahluwalia and J. Wilson, "PWSCC of Alloys 690, 52 and 152," *Proc. 13th Int. Conf. Environmental Degradation of Materials in Nuclear Power Systems – Water Reactors,* Whistler, B. C., Canadian Nuclear Society, 2007.

4. P. L. Andresen, M. M. Morra, and K. Ahluwalia, "SCC of Alloy 690 and Its Weld Metals", *ibid 2*.

5. B. Alexandreanu, "The Stress Corrosion Cracking Behavior of Alloys 690 and 152 Weld in a PWR Environment", *ibid 1.*

6. B. Alexandreanu, Y. Chen, K. Natesan, and B. Shack, "SCC Behavior of Alloy 152 in a PWR Environment", *ibid 2*.

7. B. Alexandreanu, Y. Chen, K. Natesan, and B. Shack, "Update on SCC CGR on Alloys 690/52/152 at ANL - June 2011", NRC Public Reading Room, ML111611946, 2011.

8. G. A. Young, R. A. Etien, M. J. Hackett, J. D. Tucker, T. E. Capobianco, "Physical Metallurgy, Weldability, and In-Service Performance of Nickel-Chromium Filler Metals Used in Nuclear Power Systems", *ibid 2*.

9. M. B. Toloczko and S. M. Bruemmer, "Crack-Growth Response of Alloy 690 in Simulated PWR Primary Water", *ibid 1.*

10. O.K. Chopra, W. K. Soppet, and W. J. Shack, "Effects of Alloy Chemistry, Cold Work, and Water Chemistry on Corrosion Fatigue and Stress Corrosion Cracking of Nickel Alloys and Welds", NUREG/CR-6721, 2001.

11. M. B. Toloczko, M. J. Olszta, S. M. Bruemmer, "One Dimensional Cold Rolling Effects on Stress Corrosion Crack Growth in Alloy 690 Tubing and Plate Materials", *ibid 2*.